ACS APPLIED ELECTRONIC MATERIALS

pubs.acs.org/acsaelm

Article

Smart Textile Electrochemical Capacitive Biosensor for Real-Time Monkeypox Virus Detection

Lucas F. de Lima,* Paula C. R. Corsato, Maisa A. Beluomini, André L. Ferreira, Letícia Esterdos Santos, Priscilla P. Barbosa, Camila L. Simeoni, Marcelo Bispo de Jesus, José Luiz Proenca-Modena, Thiago R. L. C. Paixão,* and William R. de Araujo*

Cite This: ACS Appl. Electron. Mater. 2025, 7, 2882−2893

Read Online

ACCESS | Metrics & More | Article Recommendations | Supporting Information

ABSTRACT: The latest outbreak caused by monkeypox virus (MPXV) has turned into an international public health emergency, underscoring the urgent need for rapid, large-scale, and sensitive diagnostic tests for MPXV. Here, a capacitive biosensor for detecting MPXV was developed using a laser-scribed graphene (LSG) sensor manufactured on synthetic aramid fiber. The aramid-LSG sensor was modified with monoclonal antibodies for detecting MPXV through electrochemical capacitance measurements (C_{μ}^{-}). The electrochemical detection was performed using a system of two interdigitated electrodes, providing excellent reproducibility and without cross-reactivity in the presence of other poxviruses and nonpoxviruses. Also, the wearable textile biosensor achieved a LOD of 7.5×10^{-1} PFU mL^{-1} and a LOQ of 2.4×10^{0} PFU mL^{-1}, enabling its application in plasma, saliva, and PBS samples (simulating application to human skin containing the virus). Furthermore, cytotoxicity assay studies demonstrated that the device is safe to use, according to the in vitro studies employing 3T3 cell cultures. This approach demonstrates the great potential of the wearable capacitive biosensor, which can be manufactured on a large scale using an environmentally friendly method for the wearable analysis of MPXV on patient skin.

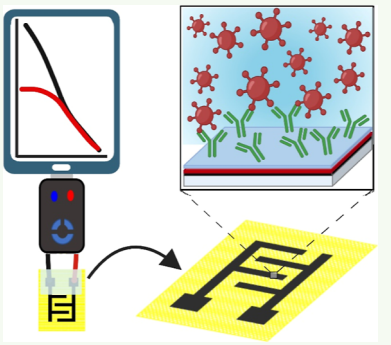

KEYWORDS: *wearable textile biosensor, laser-scribed graphene, monkeypox sensing, electrochemical biosensor, diagnosis, capacitive measurements*

1. INTRODUCTION

Wearable electrochemical biosensors have garnered significant attention in recent years due to their attractive characteristics for detecting and monitoring clinically relevant molecules in patients over extended periods of time.[1−3] These devices also have the potential to collect vital health information from the patient's body, providing valuable data that can contribute to personalized medicine.[4,5] The advantage of noninvasive and on-body monitoring conferred by wearable devices enables alerting any imminent health hazards or infections outside of the hospital environment, facilitating rapid corrective clinical action and decision-making and improving the quality of life while reducing medical costs.[6,7] From a patient's perspective, especially in remote locations or areas with limited access to physicians, the desire for on-body or minimally invasive devices for mobile health monitoring and remote diagnostics is crucial.[8] This requires using portable and miniaturized biomedical devices that can provide responses through a smartphone, enabling health monitoring and diagnostics literally at the palm of one's hand.[9] Besides, some materials are desired to be applied as wearable sensors due to their flexibility, nontoxicity, lower mechanical deformation, biocompatibility, and reproducibility.

The utilization and concept of smart textile-based wearable electrochemical sensors have been developed for over two decades.[10] These electrochemical textile (e-textiles) devices hold promise across multiple sectors, including personal protection, automotive, aerospace, and agriculture, with advancements in virtual/augmented reality and robotics that further enhance their potential for human connectivity.[11] This technology was first defined by the International Organization for Standardization as complete electronic systems integrated into textiles, opening a new avenue for the development and use of textile materials with wearable characteristics since the material presents some characteristics such as lightweight, breathable materials with flexibility, stretchability, and wash resistance.[12] These systems encompass biosensors for various measurements, data processing capabilities, and even actuation features. A classic example of the wearable textile electro-

Received: January 7, 2025
Revised: March 6, 2025
Accepted: March 10, 2025
Published: March 21, 2025

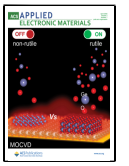

chemical sensor was created due to the COVID-19 pandemic, enabling the development of e-textiles for detecting pathogens like SARS-CoV-2, utilizing electrochemical biosensing strategies employing several methods of fabrication such as screen-printing, laser-scribed graphene (LSG), spin coating, and other technologies to manufacture wearable devices on textile surfaces.[13−15]

Due to the interesting characteristics of textiles being applicable as wearable devices for pathogen detection, a precise device fabrication method is highly desired. In response to this demand, the utilization of the LSG method can be an important tool for scalable and in situ fabrication of 3D porous graphene materials on various synthetic or natural surfaces, including paper, polyimide, poly(ether imide), and leaves, among others.[16−20] The advantages of this technique enable its scalable manufacturing of electrodes in different geometries and sizes on materials that support the photothermal conversion of the polymeric surface to a graphitic conductive material, achieved by optimizing parameters such as laser power, speed, and focal distance.[21] Additionally, the functional groups generated on the carbon surface can enhance the electrochemical performance for analyses, generating graphene-based nanomaterials rich in oxygenated functional groups and defects that produce devices with high electrocatalytic performance.[22]

By exploring the capabilities of textile materials for skin integration and leveraging the LSG technique for real-time fabrication of conductive tracks, there is compelling potential to engineer a wearable textile electrochemical biosensor specifically designed for detecting monkeypox virus (MPXV) on the skin of patients exhibiting pustules. MPXV belongs to the *Orthopoxvirus* genus of the *Poxviridae* family, exhibiting high transmissibility from human to human, primarily through sexual contact and large respiratory droplets.[23] The first mention of MPXV in humans was reported in 1970, and its infectivity has since drastically increased, reaching over 110 countries, leading the World Health Organization (WHO) to classify it as a health emergency of international concern.[24,25]

Patients with MPXV can present high viral load mainly in skin lesions (7.3 copies mL^{-1}), followed by rectal (5.0 copies mL^{-1}) and oropharyngeal samples (4.6 copies mL^{-1}),[26] which usually are detected using the gold standard method of real-time polymerase chain reaction (qPCR)[27] or other sophisticated techniques such as the CRISPR/Cas9 (clustered regularly inter spaced short palindromic repeats/CRISPR-associated protein 9) system.[28−30] Also, other methods such as lateral flow immunoassays (LFIAs),[31] loop-mediated isothermal amplification (LAMP),[32] and enzyme-linked immunosorbent assay (ELISA)[33] have already been reported in the literature for MPXV sensing. However, its methods require specialized labor to operate, costly equipment and consumables, and long periods of analysis,[34] limiting its identification in remote areas without doctors' access.

To circumvent these limitations, it is worth exploring electrochemical biosensors based on graphene electrodes modified with antibodies, utilizing a capacitive response, for wearable applications. In a recent report, Garrote et al.[35,36] have studied several quantum capacitive point-of-care (POC) devices to detect clinically relevant biomarkers for the molecular diagnosis of viruses. In the first study, a label-free capacitive POC device was developed on a gold surface for detecting the dengue virus through the NS1 protein. The electrochemical immunosensor demonstrated excellent performance in differentiating between 11 negative and 15 positive serological samples.[35] In another study, the authors reported the development of a quantum-rate-based electrochemical signal using a single layer of graphene for detecting SARS-CoV-2 infection from nasal swab specimens. The authors obtained a great performance in the presence of 12 positive and 3 negative samples, demonstrating the applicability of the POC in real samples. Despite the aforementioned studies, among other capacitive sensors reported in the literature,[35,37] there are no wearable biosensors manufactured by the LSG method using the concept of quantum capacitance.

Hence, in this work, we report a wearable electrochemical biosensor fabricated on a textile substrate of aramid using the LSG technique, modified with monoclonal antibodies for detecting MPXV on the patient's skin through capacitance measurements. The sensor exhibited excellent performance in the presence of MPXV in spiked human saliva and plasma samples, with a limit of detection (LOD) of 7.5×10^{-1} PFU mL^{-1} and a coefficient of correlation (R^2) of 0.998. Additionally, satisfactory reproducibility was achieved with relative standard deviations (RSDs) of 4.57% (n = 8 sensors) and observed noncross-reactivity in the presence of other poxviruses and nonpoxviruses, demonstrating great potential for application as a POC and a wearable sensor for detecting MPXV. The novelty of our paper lies in the development of a miniaturized electrochemical biosensor for MPXV detection, which offers a rapid, portable, and user-friendly alternative to conventional methods such as qPCR and ELISA. Despite existing approaches, our sensor enables direct detection in plasma, saliva, and skin samples with minimal preprocessing, employing a smartphone-based display for fast interpretation.

2. MATERIALS AND METHODS

2.1. Reagents and Solutions. All reagents used in this work were obtained with high analytical grade, which were previously prepared in ultrapure water (SynergyUV Water Purification System, France) with a resistivity of 18.2 MΩ cm at 25 °C. The aramid textile substrate was purchased from IMATTEC International. Phosphate buffered saline (PBS), 1-pyrenebutyric acid (PBA), bovine serum albumin (BSA), 1-ethyl-3-(3′-dimethylaminopropyl)carbodiimide hydrochloride (EDAC), and *N*-hydroxysuccinimide (NHS) were purchased from Sigma-Aldrich. MPXV A29 monoclonal antibody (IgG, Clone no. 0031) was purchased from Sino Biological. *N*,*N*-Dimethylformamide (DMF) was obtained from Synth. High-glucose Dulbecco's modified Eagle's medium (DMEM) was obtained from Vitrocell Embriolife (Brazil). Varnish (colorless shellac) used to hydrophobically apply the textile surface for LSG fabrication was obtained from Acrilex. The pooled human saliva and plasma samples (collected fresh from three donors and mixed) were purchased from Innovative Research (catalog number: IR100044P). Calcein-AM solution, DMEM, supplemented with 10% fetal bovine serum (FBS) and 1% PenStrep antibiotic and Propidium Iodide (Invitrogen) (0.025 μmol L^{-1} (1 μg mL^{-1}) and Hoechst were purchased from Invitrogen, Thermo Fisher Scientific in FluoroBrite.

2.2. Characterizations. The morphological characterization of the aramid substrate before and after the application of the LSG method was performed using scanning electron microscopy (SEM) (FEI Quanta FEG 250, field emission gun scanning electron microscope, LIMicro-IQ—Microscopy Core Facility, RRID:SCR_024633, acceleration voltage of 15 kV). Structural analysis of the LSG material obtained onto the aramid substrate was carried out by Raman spectroscopy (Horiba T64000 confocal microscope) with a 532 nm laser, 15 mW power, 30 s of exposure, and 4 scans accumulation.

The electrochemical measurements of the aramid-LSG sensor were carried out using a galvanostat/potentiostat, employing NOVA

https://doi.org/10.1021/acsaelm.5c00055
ACS Appl. Electron. Mater. 2025, 7, 2882−2893

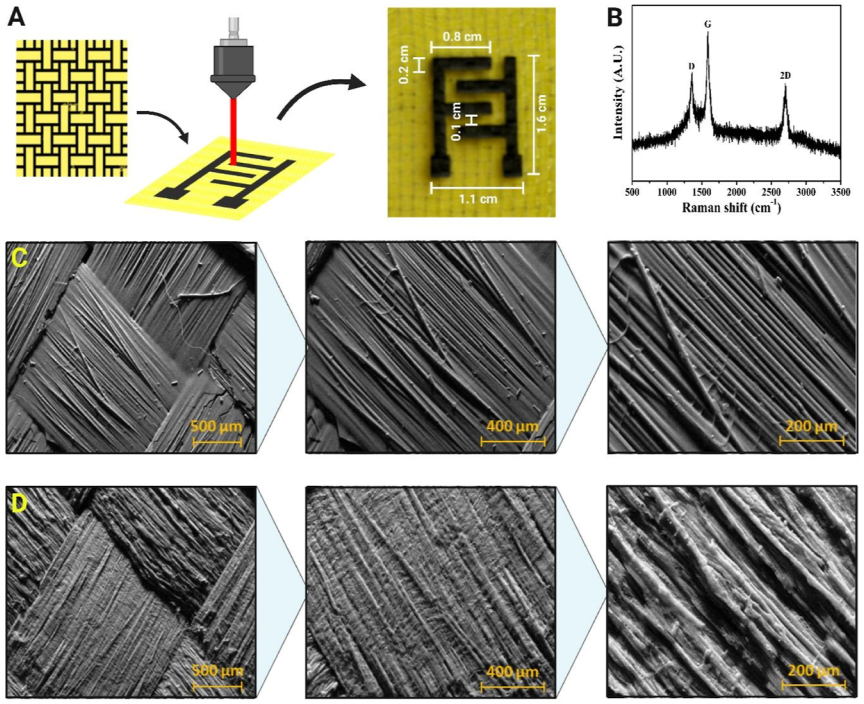

Figure 1. Fabrication and morphological characterization of the aramid-based LSG sensor. (A) Laser fabrication and respective dimensions of the aramid-LSG sensor. (B) Raman spectroscopy to the morphological LSG sensor. SEM images of the aramid surface (C) and aramid-LSG surface (D) in different magnifications. This figure was created using BioRender.com.

version 2.1.5 software. Additionally, a Sensit Smart from PalmSens with PSTrace software, connected to a Samsung A71 smartphone, was used for wearable applications of the textile electrochemical biosensor. Electrochemical impedance spectroscopy (EIS) measurements were performed in 10 mmol L^{-1} PBS (pH 7) at frequencies ranging from 1.0×10^5 to 0.1 Hz with an amplitude of 10 mV at the open-circuit potential (OCP). Complex capacitance plots were obtained from impedance data by converting impedance values into capacitance functions using the following relationship: $C^*(\omega) = 1/[j\omega Z^*(\omega)]$, where ω is the angular frequency and $j = \sqrt{-1}$. Thus, the real and imaginary components of $C^*(\omega)$ were expressed as $C' = Z''/\omega|Z|^2$ and $C'' = Z'/\omega|Z|^2$, respectively, where $|Z| = \sqrt{(Z')^2 + (Z'')^2}$ denotates the modulus of $Z^*(\omega)$, according to the Garrote et al.[36] method.

2.3. Fabrication of the Textile Wearable Sensor by CO_2 Laser Engraving. The textile LSG electrochemical sensor, manufactured on an aramid substrate by CO_2 laser engraving, was created with a system of two interdigitated electrodes (Figure 1A). Initially, the aramid substrate was fixed to a double-sided tape from 3M (30.0 cm × 30.0 cm) to facilitate CO_2 laser irradiation on a flat surface. Subsequently, the substrate was hydrophobized by spraying varnish and left to dry at room temperature for 4 h. Then, a two-electrode design (1.6 cm × 1.1 cm, with parallel plates of 0.8 cm × 0.2 cm) was created using CorelDraw software. Under optimized engraving conditions (laser engraving velocity of 30 mms^{-1} and potential of 11.5%) and with the laser output positioned 10 mm away from the paper platform, a CO_2 pulsed laser (50 W Router VS4040C, Visutec, São Paulo, Brazil) was utilized to pattern the graphene-based electrodes onto the aramid substrate (Table S1). Subsequently, the vertical parallel plates were coated with a nonconductive layer of colorless nail polish from Risque.

2.4. Biosensor Preparation and Sensing. The aramid-based LSG sensor was modified by the drop-casting method in some steps, according to the Torrente-Rodriguez et al. and De Lima et al. method with some modifications.[38,39] Briefly, 1.5 μL of 5.0 mmol L^{-1} PBA prepared in DMF was applied to each electrode and allowed to dry for 12 h at room temperature (~30 °C). Subsequently, each electrode was incubated for 30 min with 3.0 μL of a solution containing 0.4 mol L^{-1} EDAC and 0.2 mol L^{-1} NHS in 10 mmol L^{-1} PBS (pH 7.4) at room temperature (~30 °C). After this, the covalent attachment onto the activated surface was carried out through 1.5 μL of 50 μg mL^{-1} Ab-MPXV, applied to each electrode, and incubated for 3 h at room temperature. Lastly, a blocking step was performed for 90 min using 1.0 (m/v) BSA, which was previously prepared in 10 mmol L^{-1} PBS (pH 7.4).

The modified textile aramid-LSG biosensor was employed for MPXV detection in PBS, plasma, and saliva samples. For the MPXV biosensing, 100 μL of the sample containing MPXV was dropped on the interdigitated modified electrodes and incubated for 10 min at room temperature (~30 °C), according to our previous studies.[39] Afterward, the electrodic surface was rinsed with 10 mmol L^{-1} PBS (pH 7.4) to eliminate any unbound virus and other proteins, followed by the addition of an additional 100 μL of 10 mmol L^{-1} PBS (pH 7.4) for the capacitive measurements. The Z' and Z'' values derived from Nyquist plots were transformed into real capacitance (C') and imaginary capacitance (C'') values, respectively, and plotted against the log frequency values.

2.5. Reproducibility and Cross-Reactivity. A reproducibility assay was conducted using 8 biosensors manufactured from different batches. The textile LSG electrochemical immunosensors were exposed to 1×10^4 PFU/mL of MPXV and incubated for 10 min at room temperature (~30 °C). The C'' values obtained for these 8 devices were used to calculate the RSD. For cross-reactivity studies, textile electrochemical LSG biosensors were incubated for 10 min in the presence of poxvirus and nonpoxvirus strains at the same conditions used for MPXV sensing.

The inactivated virus SARS-CoV-2 B.1, SARS-CoV-2 Omicron, MPXV, Orthobunyavirus oropoucheense (OROV), Mayaro virus (MAYV), and Vaccinia virus (VACV) prepared in DMEM at 10^4 PFU/mL were used for cross-reactivity assay, and the C'' values were used to obtain the relative capacitance percentage.

2.6. Real Sample and Real-Time Analyses of MPXV. After calibrating the textile wearable LSG biosensor in 10 mmol L^{-1} PBS (pH 7.4), the biosensor was applied to detect MPXV in spiked human saliva and plasma samples. Different amounts of MPXV were spiked into the biological samples (ranging from 1×10^1 to 1×10^4 PFU mL^{-1}), followed by drop-casting 100 μL of the sample onto the

https://doi.org/10.1021/acsaelm.5c00055
ACS Appl. Electron. Mater. 2025, 7, 2882−2893

interdigitated electrodes and incubating for 10 min prior to analysis. As proof of applicability, our wearable textile LSG biosensor was used for MPXV detection on a flexible surface of PDMS, mimicking skin containing a pustule characteristic of patients diagnosed with monkeypox. For this, a PDMS surface was sprayed with MPXV using a stock solution at concentrations ranging from 1.0×10^1 to 1.0×10^4 PFU mL^{-1}. The textile wearable LSG biosensor was placed on the PDMS surface containing MPXV in PBS, and after 10 min, the measurements were recorded.

2.7. Viral Strain. This study involved the use of several viral strains, including B.1 (SARS.CoV-2/SP02.2020, GenBank accession NO. MT126808) and Omicron lineages (SARS.CoV-2 HIAE-W.A, EPI_ISL_6901961) of SARS-CoV-2, MPXV (not sequenced), Orthobunyavirus oropoucheense (OROV; isolate BeAn19991, GenBank accession no. KP052850), Mayaro virus (MAYV; isolate BeAr20290, GenBank accession no. KT754168.1), and vaccinia virus (VACV; **ATCC VR-1549**). The stocks of OROV, MAYV, and VACV were prepared in a Biosafety Level 2 Laboratory (BSL-2), while those of SARS-CoV-2 and MPXV were prepared in a Biosafety Level 3 Laboratory (BSL-3). The B.1 lineage of SARS-CoV-2 was obtained from Prof. Dr. Edison Luiz Durigon (USP), while the Omicron variant was obtained from isolate HIAE-W.A. The OROV strain was provided by Prof. Dr. Luiz Tadeu Morais Figueiredo (USP) and the VACV strain was provided by Prof. Dr. Clarice Weis Arns from the University of Campinas (UNICAMP). The MPXV was isolated from a patient in Campinas, Brazil, and confirmed by RT-qPCR.

For viral stock production, viruses were inoculated in Vero CCL81 cell monolayers, except for the Omicron variant of SARS-CoV-2, which was grown on Vero E6/TMPRSS2 cells. Titration of viral stocks was performed using plaque-forming units (PFU) assay, and the titers ranged from 1.00×10^4 PFU mL^{-1} to 2.45×10^7 PFU mL^{-1}. The viruses were inactivated using UV−C light exposure, with exposure times ranging from 1 to 15 min, depending on the virus strain. After inactivation, the viruses were stored at −80 °C until further use.

2.8. Biocompatibility and Cytotoxicity Studies. The biocompatibility and cytotoxicity of the wearable textile electrochemical biosensor was assessed using mouse embryonic fibroblasts (3T3). Cells were grown in 25 cm^2 culture flasks with DMEM, supplemented with 10% FBS and 1% PenStrep antibiotic, herein referred to as supplemented medium. Cells were subcultured every 2 d after treatment with 0.1% trypsin. During the experiments, cells were maintained at 37 °C and a 5% CO_2 atmosphere in a Panasonic COM-170AICUVL-PA incubator. The cells were maintained until 25th passage.

2.8.1. Plating and Treatment. Briefly, cells were seeded in a 96-well plate (5×10^4 cells/mL) and grown for 24 h. The sensor was placed in a 6-well plate, immersed in 3 mL of culture medium, and incubated at 37 °C, 5% CO_2, for 1 or 24 h. Subsequently, 100 μL of each treatment mixture was added to each treatment well.

2.8.2. MTT Test. MTT assay ([3-(4,5-dimethylthiazol-2-yl)-2,5-diphenyltetrazolium bromide]) determines cytotoxicity by monitoring the reduction of tetrazolium salts to formazan crystals through the oxidation of NADH in metabolically active cells. Medium from a 1 h or 24 h incubation with the sensor was used to treat the cells for 24 h; the medium was then replaced with MTT solution (1.0 mg mL^{-1}). After 90 min incubation, the medium was replaced with 100 μL DMSO to dissolve the MTT crystals. Finally, the plate was homogenized for 3 min, and the absorbance was measured at 570 nm on a Cytation 5 Imaging Multi-Mode reader (BioTek, Winooski, VT, USA). Cell viability was determined by three independent experiments ($n = 3$). Statistical difference was determined by one-way ANOVA comparing control to treatments by Dunnett's test using GraphPad Prism 8.0.2. Results were expressed as mean ± standard deviation (SD), with values normalized to the untreated cells.

2.8.3. Calcein-AM Assay. The Calcein-AM assay assesses cytotoxicity by measuring the intracellular conversion of calcein acetoxymethyl ester (Calcein-AM), a cell-permeable and non-fluorescent molecule, to calcein, a cell-impermeable and fluorescent molecule, via intracellular esterases. After 24 h of incubation, each well was incubated with 50 μL of Calcein-AM solution (0.025 μmol L^{-1}) in DMEM. After 30 min of incubation at 37 °C and 5% CO_2, the plates were analyzed using the Cytation 5 Imaging Multi-Mode Reader, with fluorescence detected at an emission wavelength of 528 nm and an excitation wavelength of 488 nm.

2.8.4. Calcein/PI/Hoechst Assay. Cell viability was also assessed by imaging using Calcein-AM, propidium iodide, and Hoechst dyes. Calcein-AM was converted into a cell-impermeable and fluorescent molecule by intracellular esterases, indicating live cells. Propidium iodide stained dead cells through intercalation with DNA, while Hoechst stained all nuclei, providing a total cell count. After 24 h of treatment, cells were stained with a solution containing Calcein-AM (0.025 μmol L^{-1}), propidium iodide (0.025 μmol L^{-1} (1 μg mL^{-1})), and Hoechst (1 μg mL^{-1}) diluted in FluoroBrite DMEM. After 30 min incubation at 37 °C and 5% CO_2, cells were imaged using the Cytation 5, capturing four different fields per well in three fluorescent channels (DAPI, PI, and GFP) at 10× magnification. Image analysis was performed using Gen5 software (3.12, BioTek Instruments) in which the stained nuclei were segmented, and the DAPI channel for Hoechst staining, representing the total number of cells, and the PI channel for propidium iodide staining, representing dead cells, were counted. The number of viable cells was calculated by subtracting the count of PI-stained nuclei from that of the Hoechst-stained nuclei. The viability percentage was determined using the equation [viable treated cells/viable control cells] × 100, providing the percentage of viable cells per well.

2.8.5. Statistical Analysis. Statistical analysis was performed using the GraphPad Prism 8.0 software (GraphPad Software, San Diego, CA). Data points are presented as mean ± SD. All experiments were repeated at least three times. After confirming that the values followed normal distribution, a two-tailed Student's t test was applied to determine the significance of the differences between two groups of independent samples. Pearson's correlation analysis was performed to determine the correlations between the two variables. The survival rate was analyzed using the Kaplan−Meier method. Statistical significance was set at $p < 0.05$. All p values are indicated in the figure ($^*p < 0.05$, ns, not significant).

3. RESULTS AND DISCUSSION

3.1. Optimizations and Characterizations of the Wearable Textile Electrochemical Sensor. The aramid-based LSG sensor was fabricated using a CO_2 laser machine, under optimized engraving conditions (laser engraving of 11 mm s^{-1} and laser power of 35%), resulting in high conductive 3D porous graphene material with lower resistance and enhanced resolution of the conductive tracks (Table S1). The design of the aramid-based LSG sensor features two parallel carbon tracks optimized to provide superior performance in capacitive measurements (Figure 1A).

Raman spectroscopy was performed to confirm the formation of graphene-based material on the flexible textile surface of the aramid. The aramid-LSG surface showed the predicted peaks for graphene materials, including the D band (~1350 cm^{-1}), attributed to structural defects in sp^2 hybridization, the G band (~1600 cm^{-1}), indicative of the stretching of sp^2 carbon bonds, and the 2D band (~2625 cm^{-1}), attributed to a resonance process, hereby offering direct evidence of the graphene formation[40] (Figure 1B). The degree of disorder was calculated by the intensity ratio of the D band to the G band, resulting in a value of 0.78. This value is consistent with the disorder induced in graphene materials by laser treatment and indicates a significant but not intense presence of structural defects.[41] To evaluate the number of graphene sheets formed, the value of I_{2D}/I_G was calculated, resulting in a value of 0.72.[42] This ratio, being lower than 1, indicates that the formed graphene consists of multilayers,

https://doi.org/10.1021/acsaelm.5c00055
ACS Appl. Electron. Mater. 2025, 7, 2882−2893

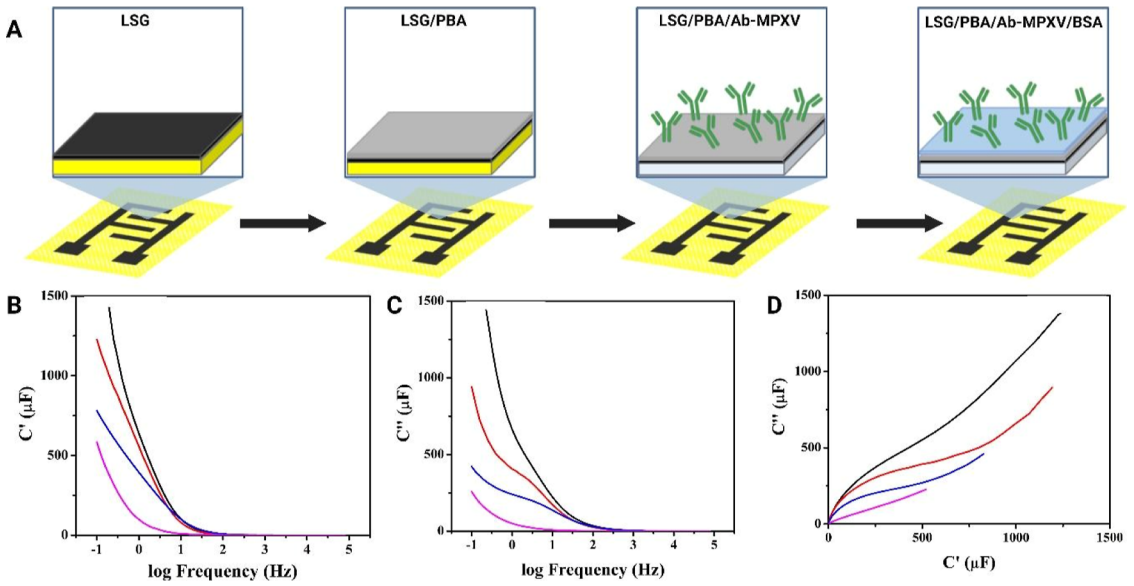

Figure 2. Characterization of each functionalization step of the disposable wearable textile electrochemical biosensor. (A) Steps of modification were performed on the interdigitated sensor manufactured on an aramid substrate by LSG and modified with PBA, Ab-MPXV, and BSA. Bode plots of the real capacitance (B) and imaginary capacitance (C) vs the log frequency. (D) Capacitive Nyquist plots. All the measurements were performed in 10 mmol L^{-1} PBS (pH 7.4), amplitude of 10 mV with a sinusoidal perturbation and frequency ranging from 1×10^5 Hz to 0.1 Hz. Legend: aramid-LSG (black line), BPA (red line), Ab-MPXV (blue line), and BSA (magenta line). This figure was created using BioRender.com.

which agrees with the current literature for LSG materials.[8,42,43]

The morphological characterizations of both the aramid and aramid-LSG was performed by SEM. The textile surface of aramid presents several fibers interwoven, to form meshes, constituting the visible surface of the fabric (Figure 1C). Following exposure to CO_2 laser engraving radiation, a noticeable increase in the roughness of the fibers was observed, which was attributed to the formation of 3D carbon tracks on the aramid surface (Figure 1D). The high porosity of the surface, associated with the lower resistance of the aramid-LSG material, presents an excellent platform for anchoring biomolecules. The electroactive area of the aramid-LSG sensors was evaluated according to the double layer capacitance measurements, which were performed by EIS in the presence of 0.1 mol L^{-1} KCl in a frequency ranging from 50 kHz to 100 Hz.[44] We obtained an electroactive area of 1.08 cm^2 for the LSG sensor. This value indicated an enhancement of 2.1-fold in the electroactive area when compared with the geometric area (0.48 cm^2) for the aramid-LSG electrode.

3.2. Design and Preparation of the Wearable Electrochemical Biosensor. To evaluate each step of the functionalization (Figure 2A), capacitive Bode plots were generated. These plots depict the logarithmic frequency-resolved impact of modifying the 3D porous graphene nanostructures obtained by LSG, showcasing changes in real and imaginary capacitive elements. Additionally, capacitive Nyquist plots were obtained (Figure 2B–D). The interdigitated textile wearable sensor underwent modification using the drop-casting method at room temperature (~30 °C). The electrochemical measurements were performed in the presence of 10 mmol L^{-1} PBS (pH7.4), and the C' and C'' values were obtained by EIS. Under optimized engraving and modification conditions, the bare LSG electrode (black line) exhibited a maximum of C' and C'' at 0 Hz of 678 and 656 μF, respectively. After the modification with PBA, C' and C'' decrease to 576 μF and 405 μF, respectively. This result is in agreement with literature reports for capacitive biosensors.[45,46] Then, the anchor of Ab-MPXV on the LSG/PBA surface drastically decreases the imaginary and real capacitance for 401 and 240 μF, respectively. Upon BSA modification, C_μ^- decreased to 103 μF and 59 μF, confirming the blocking of the nonspecific sites present on the LSG surface. The consistent reduction of both C' and C'' following each modification step is attributed to the adsorption or formation of covalent bonds between (bio)molecules and the nanostructured LSG surface.[45] These results suggest that the aramid-LSG electrode holds promise as a potential transducer platform for manufacturing wearable biosensors. Besides, the capacitive Nyquist plots show the changes of real and imaginary capacitive elements.

The C_μ^- values are highly dependent on the density of states (DOS). Consequently, biorecognition events on the modified biosensor generate electronic DOS perturbations, leading to a decrease in C' values in accordance with the respective target concentration. Moreover, the C'' values decrease in the same trend as C', corroborating the findings reported in the literature.[47,48]

3.3. Electroanalytical Performance, Reproducibility, and Cross-Reactivity of the Wearable Electrochemical Biosensor. The transduction mechanism of our device depends on changes in the electrochemical capacitance when the target binds to the biological receptor anchored on the working electrode.[49] Additionally, the graphene-based material generated after the photothermal process of laser irradiation on polymeric materials may contribute to capacitance, attributed to localized and nonlocalized electronic states.[45] Capacitance is determined using impedance-derived electrochemical capacitance spectroscopy, a method introduced approximately 10 years ago and widely explored in the biological recognition of biomarkers, particularly for POC devices.[36] Besides, the electrochemical capacitance (C_μ^-) has been used effectively as a transducer signal in biological interfaces and can be expressed as a series of its nonfaradaic (C_i) and quantum or faradaic (C_q)

https://doi.org/10.1021/acsaelm.5c00055
ACS Appl. Electron. Mater. 2025, 7, 2882−2893

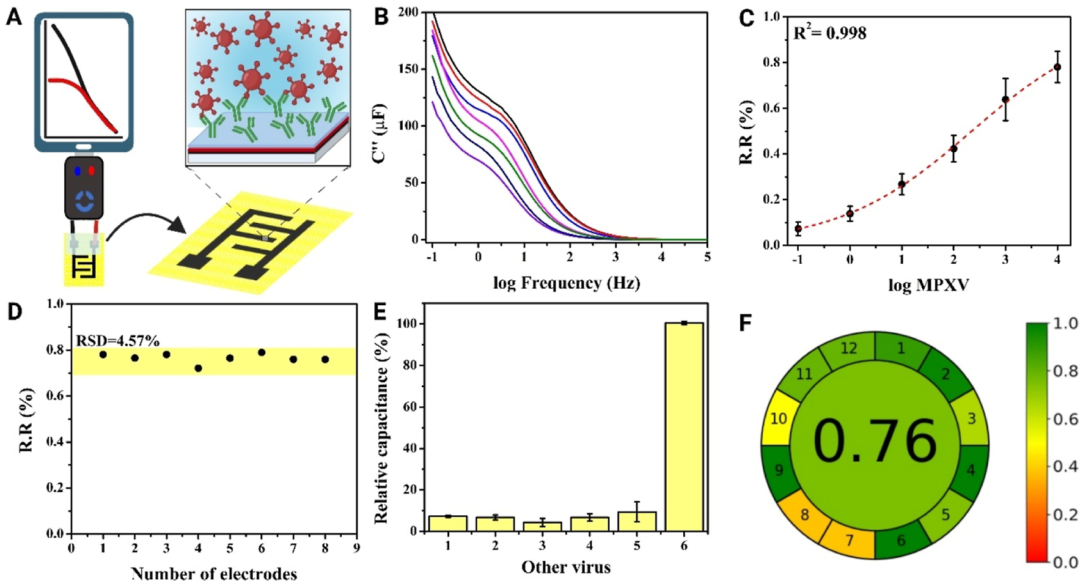

Figure 3. (A) Schematic representation of MPXV capacitive electrochemical detection using the LSG/Ab-MPXV/BSA biosensor, using a portable potentiostat and a smartphone. (B) Capacitive imaginary plots from Bode data for MPXV concentrations ranging from 1.0×10^4 to 1.0×10^{-1} PFU mL^{-1} in 10 mmol L^{-1} PBS (pH 7.4). (C) Normalized capacitive values extracted from the measurements performed in Figure 3A of the logarithm of the MPXV concentration. (D) Reproducibility assays performed using 8 different sensors (n = 8) in the presence of 1.0×10^4 PFU mL^{-1} MPXV in 10 mmol L^{-1} PBS (pH 7.4). (E) Cross-reactivity studies using LSG/Ab-MPX/BSA in the presence of poxvirus and nonpoxvirus strains. (1) Vaccinia virus, (2) SARS-CoV-2 (omicron variant), (3) SARS-CoV-2 (B.1 variant), (4) Orthobunyavirus oropoucheense, (5) alphavirus Mayaro, and (6) MPXV (all at 10^4 PFU mL^{-1}). (F) Analytical GREEness Metric approach (AGREE) of our LSG/Ab-MPX/BSA, indicating that our procedure presents a scale of 0.76. The error bars represent the SD of the measurements, which were performed in triplicate (n = 3). This figure was created using BioRender.com.

components, i.e., a concise equation (eq 1) can be expressed as summarizing the information

$$\frac{1}{C_\mu^-} = \frac{1}{C_i} + \frac{1}{C_q} \tag{1}$$

C_i represents the double-layer capacitance, whereas C_q is associated with the occupancy of accessible quantum states at the interface and is directly proportional to the electronic DOS, as observed in graphene.[46] When considering nanostructured interfaces, for example rGO or GO, $C_i \gg C_q$, enabling that quantum capacitance component governs the overall electrochemical capacitance, which lead to $C_\mu^- \approx C_q$.[35] Thus, C_μ^- can serve as a viable option for signal transduction in biosensors as its DOS is sensitive to alterations in the dielectric environment caused by receptor-molecular target biorecognition events taking place at the electrode/electrolyte interface.

For the electrochemical detection of MPXV employing the LSG/Ab-MPXV/BSA biosensor, the changes in the imaginary capacitance values from Bode plots obtained by EIS measurements at a fixed frequency of 0 Hz were evaluated. For this purpose, varying amounts of MPXV on 10 mmol L^{-1} of PBS were initially assessed. The binding between Ab-MPXV immobilized onto the electrode surface and MPXV induced changes in the capacitance response, demonstrating a correlation with the target for analytical purposes.[50]

The changes in $\frac{1}{C_\mu^-}$ were quantified according to the percentage of relative variation of the electrochemical capacitance signal, which was expressed in the following equation[45]

$$\mathrm{RR}\ (\%) = \left[\left(\frac{\frac{1}{C_\mu^-\ (\mathrm{target})} - \frac{1}{C_\mu^-\ (\mathrm{blank})}}{\frac{1}{C_\mu^-\ (\mathrm{blank})}}\right)\right] \times 100 \tag{2}$$

where $\frac{1}{C_\mu^-\ (\mathrm{target})}$ is the value of the inverse of electrochemical capacitance after the incubation with MPXV sample, and $\frac{1}{C_\mu^-\ (\mathrm{blank})}$ is the value of the inverse of electrochemical capacitance in the presence of the medium without the target (PBS, saliva, plasma).

Under optimized functionalization conditions, antibody amounts, and incubation times, the developed biosensor can detect MPXV in a miniaturized and wearable system with adequate analytical performance. This can be achieved in the palm of the operator's hand using a portable potentiostat and a smartphone (Figure 3A). For electrochemical detection of MPXV, C'' from Bode plots with normalized values were obtained to quantify the targets. According to the Bode capacitive plots in Figure 3B, the capacitance values decrease with the increase in the concentration of the target ranging from 1.0×10^{-1} to 1.0×10^4 PFU mL^{-1} in 10 mmol L^{-1} PBS (pH 7.4), resulting in a determination coefficient (R^2) of 0.998 (Figure 3C). The signal response curve follows a logarithmic relationship, which is typical in biosensors. At lower concentrations of the mpox virus, small changes in concentration cause significant changes in the signal. As the concentration increases, the response becomes less sensitive, reaching a saturation point. This behavior reflects the sensor's high sensitivity at low concentrations, making it effective for early detection.

The LOD was calculated according to the 4PL method,[51] and the LOQ was calculated using the IUPAC method.[52] We

https://doi.org/10.1021/acsaelm.5c00055
ACS Appl. Electron. Mater. 2025, 7, 2882−2893

Table 1. Comparison of the Analytical Parameters Obtained for Our LSG/Ab-MPXV/BSA Biosensor and the Reports in the Literature for MPXV Detection[a]

method	LOD	technique	interval range	real sample	references
CFP/MoO_3−CQDs/Ab-A29/BSA	0.5×10^{-9} mol L^{-1}	DPV	0.5×10^{-9} to 1.0×10^{-6} mol L^{-1}	serum	56
LSG/AuNS/Ab-MPXV/BSA	7.8×10^{-3} PFU mL^{-1}	EIS	1.0×10^{-1} to 1.0×10^{4} PFU mL^{-1}	plasma and saliva	17
LAMP	5.0×10^{-2} copies/μL	MCDA	1.2×10^{-3} to 1.2×10^{-2} copies per reaction	blood	57
LFB	5.0×10^{-11} g mL^{-1} for purified A29	colorimetric	2.0×10^{-11} to 2.0×10^{-7} g mL^{-1}	saliva	58
our method	**7.5×10^{-1} PFU mL^{-1}**	**capacitance**	**1.0×10^{-1} to 1.0×10^{4} PFU mL^{-1}**	**pustule, plasma and saliva**	**this work**

[a]Legend: LAMP: loop-mediated isothermal amplification; MCDA: multiple cross displacement amplification; LFB: lateral flow biosensor; CFP: carbon fiber paper; MoO_3: molybdenum oxide; CQRs: luminescent carbon quantum dots.

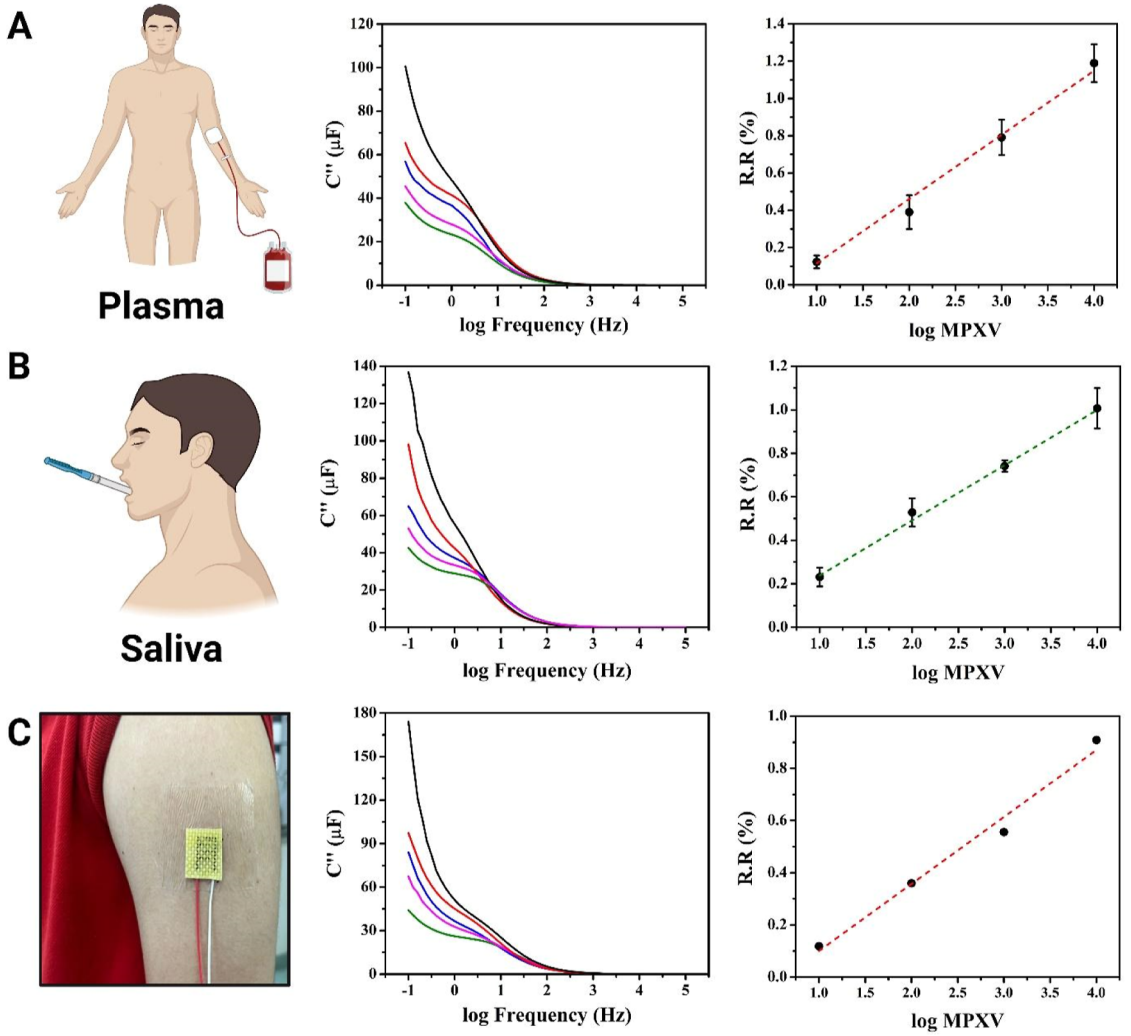

Figure 4. Electrochemical detection of MPXV in real samples employing the LSG/Ab-MPXV/BSA biosensor. (A) Analyses of MPXV in a human plasma sample. (B) Analyses of MPXV in a human saliva sample. (C) MPXV using the wearable textile biosensor. All the measurements were performed in the presence of MPXV at concentrations ranging from 1×10^{1} to 1×10^{4} PFU mL^{-1} by capacitance. Legend: (black ●) blank, (red ●) 1.0×10^{1} PFU mL^{-1}, (blue ●) 1.0×10^{2} PFU mL^{-1}, (pink ●) 1.0×10^{3} PFU mL^{-1}, (green ●) 1.0×10^{4} PFU mL^{-1}. This figure was created using BioRender.com.

obtained a LOD and LOQ of 7.5×10^{-1} PFU mL^{-1} and 2.4×10^{0} PFU mL^{-1}, respectively. These parameters are significant for the clinical tests evaluated for MPXV sensing in all the biological fluids samples.[25,26,53] They demonstrate that the wearable textile electrochemical biosensor presented a great performance in detecting MPXV in PBS medium.[53,54]

Reproducibility studies were conducted using eight (n = 8) LSG/Ab-MPXV/BSA biosensors in the presence of 1.0×10^{4} PFU mL^{-1} MPXV in 10 mmol L^{-1} PBS medium. A RSD of 4.57% was achieved, indicating excellent reproducibility for the biosensor (Figure 3D). This result, combined with the scalable method of LSG fabrication, facilitates the production of disposable, high-frequency, and rapid tests for MPXV. Cross-

https://doi.org/10.1021/acsaelm.5c00055
ACS Appl. Electron. Mater. 2025, 7, 2882−2893

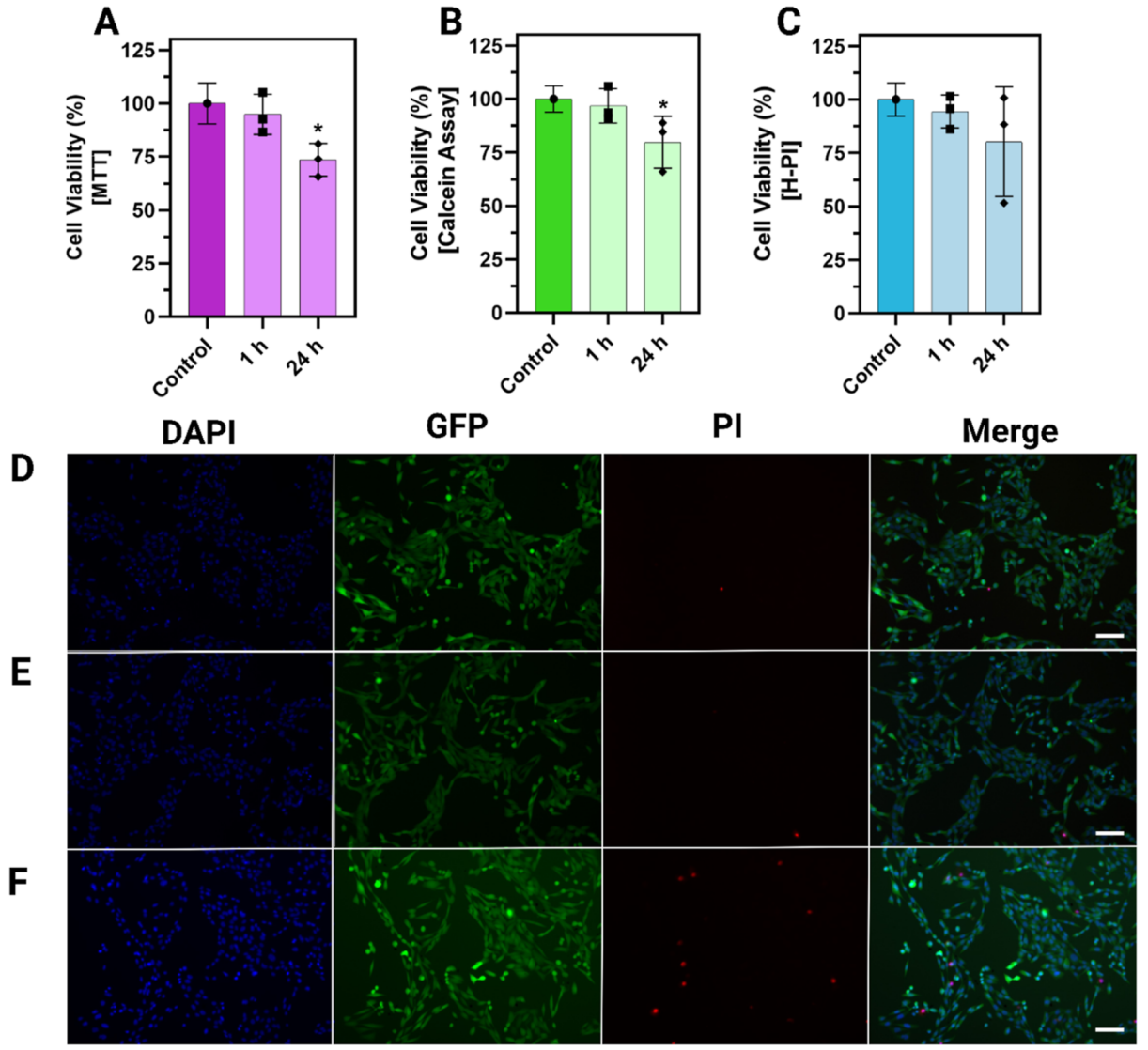

Figure 5. Cytotoxicity profile of the wearable electrochemical biosensor on 3T3 embryonic fibroblast cells. Cytotoxicity was determined using (A) MTT assay, (B) Calcein assay, and (C) Hoechst−PI analysis. Representative images of cells labeled with Hoechst (DAPI channel), Calcein (GFP channel), and propidium iodide (PI channel) are shown for (D) control cells, (E) cells exposed for 1 h, and (F) cells exposed for 24 h. Data are normalized with the control set as 100%. The points on the graph represent the means and SDs of three experiments. * = when p value > 0.05. This figure was created using BioRender.com.

reactivity assays were performed using the capacitive electrochemical biosensor in the presence of another poxvirus (vaccinia virus) and nonpoxviruses [SARS-CoV-2 (Omicron variant), SARS-CoV-2 (B.1 variant), Orthobunyavirus oropoucheense, and alphavirus Mayaro virus] in the presence of 1.0×10^4 PFU mL^{-1} MPXV in 10 mmol L^{-1} PBS medium. The experiments were conducted under the same conditions as those used for MPXV quantification. Figure 3E demonstrates that the LSG/Ab-MPXV/BSA biosensor exhibits no cross-reactivity with other viruses (>10%), underscoring its excellent selectivity and positioning it as a powerful tool for MPXV detection.

Another advantage of the developed biosensor is its eco-friendly characteristic, which was assessed through the 12 principles of green chemistry using the Analytical GREEness Metric approach (AGREE) and transformed into a unified scale from 0 to 1.[55] A score of 0.76 (green color) was obtained, indicating that the evaluated procedure is environmentally friendly and safe for humans and the environment (Figure 3F). The excellent analytical performance, associated with the environmentally friendly nature of the device and its miniaturized features, opens a new possibility for the development of portable, miniaturized, disposable, and wearable devices manufactured by the LSG technique on textile substrates for capacitance measurements of MPXV. Additionally, the stability of the biosensor was tested over 10 days when stored at 4 °C in Petri dishes, showing that its sensitivity is significantly affected after 5 days (Figure S2).

Considering that the present work reports the first wearable textile biosensor fabricated by the LSG technique for MPXV detection, a comparison was made between the proposed method and other methods described in the literature (Table 1). The parameters analyzed in this comparative study included the LOD, technique employed, and linear range. Among the works mentioned in Table 1, the biosensor presented in this work exhibits superior characteristics, including an LOD, environmental friendliness, and ease of use for POC analysis.

https://doi.org/10.1021/acsaelm.5c00055
ACS Appl. Electron. Mater. 2025, 7, 2882−2893

3.4. MPXV Evaluation in Biological Samples and Real Time. As proof of the applicability of the proposed method for MPXV detection, the LSG/Ab-MPXV/BSA biosensor was employed to quantify MPXV in human saliva and plasma samples. These biological fluids were spiked with different amounts of MPXV, ranging from low to intermediate viral loads.[53,54] The biological samples were spiked with MPXV at concentrations ranging from 1.0×10^{-1} PFU mL^{-1} to 1.0×10^{4} PFU mL^{-1} without pretreatment. The analysis protocol was the same as that employed for MPXV quantification in PBS, and the capacitance measurements were recorded using 10 mmol L^{-1} PBS (pH 7.4). Figure 4 shows the results obtained using the modified LSG/Ab-MPXV/BSA biosensor analyzing MPXV in plasma (Figure 4A) and saliva (Figure 4B). The sensitivity values (slopes) obtained from the analytical curves for PBS, saliva, and plasma samples were compared, resulting in values of 0.174 ± 0.007 for PBS, 0.254 ± 0.010 for saliva, and 0.345 ± 0.019 for plasma, as shown in Figure S1. These results demonstrate that there is a matrix effect for the plasma sample compared to PBS due to the variations on C_{μ}^{-} response. The matrix effect for plasma and saliva samples was already anticipated since the complexity of this sample presented a significant consideration in analytical chemistry and clinical diagnostics. Plasma and saliva matrix are rich in proteins, hormones, electrolytes, glucose, and other dissolved substances that can cause nonspecific binding and variations in ionic strength.[37,59] It is important to highlight that no pretreatment of the sample was carried out for the application of the biosensor developed in this work. Different samples of varying complexities were used to demonstrate their potential application. Thus, the biosensor application can be directed toward each type of biological matrix such as urine, semen, plasma, saliva, stool, and oropharyngeal swab and for each individual.

The biosensor was integrated with a portable potentiostat and a smartphone to assess the feasibility of the wearable textile electrochemical biosensor for real-time analyses on patient skin. This setup allowed for the electrochemical response of MPXV on a surface mimicking human skin (Figure 4C). To simulate this, a PDMS surface (1 × 1 cm) was drop-cast with 100 μL of MPXV solution prepared in 10 mmol L^{-1} PBS (pH 7.4). The sampling procedure involved placing the wearable textile biosensor on the PDMS surface containing MPXV for 10 min, followed by capacitive measurements. Subsequently, capacitive measurements were obtained across a range of minimum test concentrations from 1.0×10^{-1} to 1.0×10^{4} PFU mL^{-1}, demonstrating the favorable performance of the wearable biosensor. For a real application on human skin, the wearable textile biosensor can be composed of a layer containing agar prepared in PSB or the human sweat can be used as an electrolyte for the electrochemical measurements in situ.

Despite its simplicity, the wearable textile biosensor facilitates the rapid identification of MPXV in various matrices and directly on the user, offering a swift response. Associated with the method's environmentally friendly and scalable characteristics, it has the potential to serve as a powerful tool for rapid screening and real-time analysis of MPXV. Also, when compared with traditional methods of PCR, ELISA, and LAMP, electrochemical biosensors present several advantages that can be compared in Table S2.

3.5. Biocompatibility and Cytotoxicity of the Wearable Textile Electrochemical Biosensor. To estimate the cytotoxicity of the wearable biosensor on users, MTT and Calcein assays were performed in addition to image staining with Calcein, PI, and Hoechst. An overview of the cytotoxicity profile of the wearable electrochemical biosensor on 3T3 embryonic fibroblast cells is presented in Figure 5. No signs of cytotoxicity were observed in 3T3 fibroblast cells after a 1 h exposure to the electrochemical biosensor. The MTT assay (Figure 5A) revealed a reduction of 5.16% in cell viability, Calcein-AM assay showed a 3.17% reduction (Figure 5B), and the Hoechst−PI indicated a 5.56% reduction (Figure 5 C). For cells incubated for 24 h, MTT and Calcein-AM assays reported a significant decrease in cell viability of 21.2% and 16.9%, respectively (Figure 5A,B). No cytotoxicity was observed in image analysis or visual inspection of cell morphology, suggesting that the reductions observed in the MTT and Calcein-AM assays affected only a small population of cells (Figure 5A−C). Considering that the device is intended for use for about 15 min (10 min for incubation and 5 min for analysis) and based on the toxicity tests conducted at different time points (1 and 24 h), we can affirm that the electrochemical biosensor exhibits low cytotoxicity in short-term applications, thereby minimizing the risk of cytotoxicity.

Due to the applicability of the developed device as a wearable sensor, cytotoxicity assays were performed to assess the device's safety. According to the cytotoxicity results obtained (Figure 5), the wearable electrochemical biosensor manufactured on an aramid textile substrate by the LSG technique, modified with monoclonal antibodies for detecting MPXV on patient' s skin through capacitance measurements, is a potential tool to be applied without toxicity problems to the user. This study allows significant advances in clinical testing and wearable sensing since many studies reported in the literature do not evaluate the cytotoxicity effect of the sensing device.

4. CONCLUSIONS

In this study, we pioneered the development of a novel electrochemical capacitive biosensor by fabricating a high-strength synthetic fiber (aramid substrate) using CO_2 laser engraving in an electrochemical system of two interdigitated electrodes. The aramid-LSG substrate, created by the LSG technique, was modified with monoclonal antibodies to detect MPXV through capacitance measurements. The biosensor showed excellent reproducibility without cross-reactivity in the presence of other poxviruses and nonpoxviruses. The wearable textile biosensor, although simple, facilitates the rapid identification of MPXV in various matrices and directly on the user, offering a swift response. Furthermore, cytotoxicity assay studies demonstrated that the device can be used safely by the user. The sensor was applied to plasma, saliva, and PBS samples (simulating application to human skin containing the virus), demonstrating great potential for application as a POC and wearable sensor for the real-time analysis of MPXV on patient skin. Furthermore, due to its eco-friendly characteristics, our biosensor was designed for single-use only, i.e., one device per measurement. As a future direction, we aim to improve the stability of the biosensor to extend its usability over a longer period.

■ ASSOCIATED CONTENT

Supporting Information

The Supporting Information is available free of charge at https://pubs.acs.org/doi/10.1021/acsaelm.5c00055.

https://doi.org/10.1021/acsaelm.5c00055
ACS Appl. Electron. Mater. 2025, 7, 2882−2893

Matrix effect of the electrochemical biosensor, biosensor stability at 4 °C, laser engraving parameters on the aramid substrate, and comparison of biosensors for monkeypox detection with the others reported in the literature (PDF)

AUTHOR INFORMATION

Corresponding Authors

Lucas F. de Lima − *Departamento de Química Fundamental, Instituto de Química, Universidade de São Paulo, São Paulo, São Paulo 05508-000, Brasil; Laboratório de Sensores Químicos Portáteis, Departamento de Química Analítica, Instituto de Química, Universidade Estadual de Campinas—UNICAMP, Campinas, São Paulo 13083-970, Brazil;* orcid.org/0000-0001-9734-7251; Email: delimalf@unicamp.br

William R. de Araujo − *Laboratório de Sensores Químicos Portáteis, Departamento de Química Analítica, Instituto de Química, Universidade Estadual de Campinas—UNICAMP, Campinas, São Paulo 13083-970, Brazil;* orcid.org/0000-0001-5846-4236; Email: wra@unicamp.br

Thiago R. L. C. Paixão − *Departamento de Química Fundamental, Instituto de Química, Universidade de São Paulo, São Paulo, São Paulo 05508-000, Brasil;* orcid.org/0000-0003-0375-4513; Email: trlcp@iq.usp.br

Authors

Paula C. R. Corsato − *Laboratório de Sensores Químicos Portáteis, Departamento de Química Analítica, Instituto de Química, Universidade Estadual de Campinas—UNICAMP, Campinas, São Paulo 13083-970, Brazil*

Maisa A. Beluomini − *Laboratório de Sensores Químicos Portáteis, Departamento de Química Analítica, Instituto de Química, Universidade Estadual de Campinas—UNICAMP, Campinas, São Paulo 13083-970, Brazil; Faculdade de Ciências Agrárias e Veterinárias, Universidade Estadual Paulista (UNESP), Jaboticabal, São Paulo 14870-260, Brasil*

André L. Ferreira − *Nano-Cell Interactions Lab., Departamento de Bioquímica e Biologia Tecidual, Instituto de Biologia, Universidade Estadual de Campinas, Campinas, São Paulo 13083-862, Brasil*

Letícia Esterdos Santos − *Nano-Cell Interactions Lab., Departamento de Bioquímica e Biologia Tecidual, Instituto de Biologia, Universidade Estadual de Campinas, Campinas, São Paulo 13083-862, Brasil*

Priscilla P. Barbosa − *Laboratório de Estudos de Vírus Emergentes, Departamento de Genética, Evolução, Microbiologia e Imunologia and Cluster de Pesquisa Em Medicina Experimental, Universidade Estadual de Campinas, Campinas, São Paulo 13083-862, Brasil*

Camila L. Simeoni − *Laboratório de Estudos de Vírus Emergentes, Departamento de Genética, Evolução, Microbiologia e Imunologia and Cluster de Pesquisa Em Medicina Experimental, Universidade Estadual de Campinas, Campinas, São Paulo 13083-862, Brasil*

Marcelo Bispo de Jesus − *Nano-Cell Interactions Lab., Departamento de Bioquímica e Biologia Tecidual, Instituto de Biologia, Universidade Estadual de Campinas, Campinas, São Paulo 13083-862, Brasil;* orcid.org/0000-0003-0812-1491

José Luiz Proenca-Modena − *Laboratório de Estudos de Vírus Emergentes, Departamento de Genética, Evolução, Microbiologia e Imunologia and Cluster de Pesquisa Em Medicina Experimental, Universidade Estadual de Campinas, Campinas, São Paulo 13083-862, Brasil;* orcid.org/0000-0002-4996-3153

Complete contact information is available at: https://pubs.acs.org/10.1021/acsaelm.5c00055

Funding

The Article Processing Charge for the publication of this research was funded by the Coordenacao de Aperfeicoamento de Pessoal de Nivel Superior (CAPES), Brazil (ROR identifier: 00x0ma614).

Notes

The authors declare no competing financial interest.

ACKNOWLEDGMENTS

We are thankful to the Brazilian agencies Coordenação de Aperfeiçoamento de Pessoal de Nível Superior—Brasil (CAPES) (Finance Code 001; grant number: 88887.661921/2022-00), FAPESP (grant numbers: 2018/08782-1, 2023/12589-0, 2022/03250-7, 2023/00246-1, 2022/00723-1, 2022/10442-0, 2022/00723-1), and CNPq (grant number: 405620/2021-7, 310282/2022-5, 302839/2020-8) for supporting this work. JLPM is supported by the CNPq, grant number: 309971/2023-3.

REFERENCES

(1) Chen, C.; Zhou, J.; Li, Z.; Xu, Y.; Ran, T.; Gen, J. Wearable Electrochemical Biosensors for In Situ Pesticide Analysis from Crops. *J. Electrochem. Soc.* **2023**, *170* (11), 117512.

(2) Bian, S.; Zhu, B.; Rong, G.; Sawan, M. Towards Wearable and Implantable Continuous Drug Monitoring: A Review. *J. Pharm. Anal.* **2021**, *11* (1), 1−14.

(3) Wang, M.; Yang, Y.; Min, J.; Song, Y.; Tu, J.; Mukasa, D.; Ye, C.; Xu, C.; Heflin, N.; McCune, J. S.; Hsiai, T. K.; Li, Z.; Gao, W. A Wearable Electrochemical Biosensor for the Monitoring of Metabolites and Nutrients. *Nat. Biomed. Eng.* **2022**, *6* (11), 1225−1235.

(4) Yang, Y.; Gao, W. Wearable and Flexible Electronics for Continuous Molecular Monitoring. *Chem. Soc. Rev.* **2019**, *48*, 1465−1491.

(5) Teymourian, H.; Parrilla, M.; Sempionatto, J. R.; Montiel, N. F.; Barfidokht, A.; Van Echelpoel, R.; De Wael, K.; Wang, J. Wearable Electrochemical Sensors for the Monitoring and Screening of Drugs. *ACS Sens.* **2020**, *5* (9), 2679−2700.

(6) Hong, W.; Lee, W. G. Wearable Sensors for Continuous Oral Cavity and Dietary Monitoring toward Personalized Healthcare and Digital Medicine. *Analyst* **2020**, *145* (24), 7796−7808.

(7) Baldo, T. A.; de Lima, L. F.; Mendes, L. F.; de Araujo, W. R.; Paixão, T. R. L. C.; Coltro, W. K. T. Wearable and Biodegradable Sensors for Clinical and Environmental Applications. *ACS Appl. Electron. Mater.* **2021**, *3* (1), 68−100.

(8) de Lima, L. F.; Ferreira, A. L.; de Araujo, W. R. Sensing Interfaces: Materials for Wearable Sensors. *Encyclopedia of Sensors and Biosensors*; Elsevier, 2023; Vol. *1*−*4*, pp 636−649.

(9) Su, H.; Sun, F.; Lu, Z.; Zhang, J.; Zhang, W.; Liu, J. A Wearable Sensing System Based on Smartphone and Diaper to Detect Urine In-Situ for Patients with Urinary Incontinence. *Sensor. Actuator. B Chem.* **2022**, *357* (November 2021), 131459.

(10) Jung, M.; Jeon, S.; Bae, J. Scalable and Facile Synthesis of Stretchable Thermoelectric Fabric for Wearable Self-Powered Temperature Sensors. *RSC Adv.* **2018**, *8* (70), 39992−39999.

(11) Sankauskaite, A.; Pauliukaite, R.; Baltusnikaite-Guzaitiene, J.; Abraitiene, A. Smart Textile with Integrated Wearable Electrochemical Sensors. *Curr. Opin. Electrochem.* **2023**, *42*, 101410.

(12) Simegnaw, A. A.; Malengier, B.; Rotich, G.; Tadesse, M. G.; Van Langenhove, L. Review on the Integration of Microelectronics for E-Textile. *Materials* **2021**, *14* (17), 5113.
(13) Adeel, M.; Asif, K.; Alshabouna, F.; Canzonieri, V.; Rahman, M. M.; Ansari, S. A.; Güder, F.; Rizzolio, F.; Daniele, S. Label-Free Electrochemical Aptasensor for the Detection of SARS-CoV-2 Spike Protein Based on Carbon Cloth Sputtered Gold Nanoparticles. *Biosens. Bioelectron.:X* **2022**, *12* (September), 100256.
(14) Kaushik, A. K.; Dhau, J. S.; Gohel, H.; Mishra, Y. K.; Kateb, B.; Kim, N.-Y.; Goswami, D. Y. Electrochemical SARS-CoV-2 Sensing at Point-of-Care and Artificial Intelligence for Intelligent COVID-19 Management. *ACS Appl. Bio Mater.* **2020**, *3* (11), 7306−7325.
(15) Eissa, S.; Al-Kattan, K.; Zourob, M. Combination of Carbon Nanofiber-Based Electrochemical Biosensor and Cotton Fiber: A Device for the Detection of the Middle-East Respiratory Syndrome Coronavirus. *ACS Omega* **2021**, *6* (47), 32072−32080.
(16) Mendes, L. F.; Pradela-Filho, L. A.; Paixão, T. R. L. C. Polyimide Adhesive Tapes as a Versatile and Disposable Substrate to Produce CO2 Laser-Induced Carbon Sensors for Batch and Microfluidic Analysis. *Microchem. J.* **2022**, *182* (July), 107893.
(17) de Lima, L. F.; Barbosa, P. P.; Simeoni, C. L.; de Paula, R. F.; Proenca-Modena, J. L.; de Araujo, W. R. Electrochemical Paper-Based Nanobiosensor for Rapid and Sensitive Detection of Monkeypox Virus. *ACS Appl. Mater. Interfaces* **2023**, *15* (50), 58079−58091.
(18) de Lima, L. F.; de Araujo, W. R. Laser-Scribed Graphene on Polyetherimide Substrate: An Electrochemical Sensor Platform for Forensic Determination of Xylazine in Urine and Beverage Samples. *Microchim. Acta* **2022**, *189* (12), 465.
(19) de Araujo, W. R.; Frasson, C. M. R.; Ameku, W. A.; Silva, J. R.; Angnes, L.; Paixão, T. R. L. C. Single-Step Reagentless Laser Scribing Fabrication of Electrochemical Paper-Based Analytical Devices. *Angew. Chem., Int. Ed.* **2017**, *56* (47), 15113−15117.
(20) Crapnell, R. D.; Bernalte, E.; Muñoz, R. A. A.; Banks, C. E. Electroanalytical Overview: The Use of Laser-Induced Graphene Sensors. *Anal. Methods* **2025**, *17* (4), 635−651.
(21) Silva-Neto, H. A.; de Lima, L. F.; Rocha, D. S.; Ataide, V. N.; Meloni, G. N.; Moro, G.; Raucci, A.; Cinti, S.; Paixão, T. R. L. C.; de Araujo, W. R.; Coltro, W. K. T. Recent Achievements of Greenness Metrics on Paper-Based Electrochemical (Bio) Sensors for Environmental and Clinical Analysis. *TrAC, Trends Anal. Chem.* **2024**, *174* (June 2023), 117675.
(22) Lin, J.; Peng, Z.; Liu, Y.; Ruiz-Zepeda, F.; Ye, R.; Samuel, E. L. G.; Yacaman, M. J.; Yakobson, B. I.; Tour, J. M. Laser-Induced Porous Graphene Films from Commercial Polymers. *Nat. Commun.* **2014**, *5*, 5−12.
(23) Stefano, J. S.; Silva, L. R. G. e.; Kalinke, C.; Crapnell, P. R.; Brazaca, L. C.; Bonacin, J. A.; Campuzano, S.; Banks, C. E.; Janegitz, B. C.; Janegitz, B. C. Human Monkeypox Virus: Detection Methods and Perspectives for Diagnostics. *TrAC, Trends Anal. Chem.* **2023**, *167* (February), 117226.
(24) Colavita, F.; Antinori, A.; Nicastri, E.; Focosi, D.; Girardi, E.; Vaia, F.; Maggi, F. Monkeypox Virus in Human Body Sites and Fluids: Evidence for Transmission. *Lancet Infect. Dis.* **2023**, *23* (1), 6−8.
(25) Hernaez, B.; Muñoz-Gómez, A.; Sanchiz, A.; Orviz, E.; Valls-Carbo, A.; Sagastagoitia, I.; Ayerdi, O.; Martín, R.; Puerta, T.; Vera, M.; Cabello, N.; Vergas, J.; Prieto, C.; Pardo-Figuerez, M.; Negredo, A.; Lagarón, J. M.; del Romero, J.; Estrada, V.; Alcamí, A. Monitoring Monkeypox Virus in Saliva and Air Samples in Spain: A Cross-Sectional Study. *Lancet Microbe* **2023**, *4* (1), e21−e28.
(26) Suñer, C.; Ubals, M.; Tarín-Vicente, E. J.; Mendoza, A.; Alemany, A.; Hernández-Rodríguez, A.; Casañ, C.; Descalzo, V.; Ouchi, D.; Marc, A.; Rivero, A.; Coll, P.; Oller, X.; Cabrera, J. M.; Vall-Mayans, M.; Folgueira, M. D.; Melendez, M. A.; Agud-Dios, M.; Gil-Cruz, E.; de Leon, A. P.; Marinero, A. R.; Buhiichyk, V.; Galván-Casas, C.; Paredes, R.; Prat, N.; Farre, M.-R. S.; Bonet-Simó, J. M.; Farré, M.; Ortiz-Romero, P. L.; Clotet, B.; García-Patos, V.; Casabona, J.; Guedj, J.; Cardona, P.-J.; Blanco, I.; Marks, M.; Mitjà, O.; Santos, J. R.; Bailón, L.; Benet, S.; Andres, J. A.; Lozano, L. C.; Díaz, M. C.; Serrano, C. B.; Galán, E. C.; Manzano, A. I. P.; Rabadán, P. N.; Muntané, L.; Doncel, C. S.-L.; Pueo, Y. M. M.; Quinto, A. M.; Acosta, M.; Alvarez, P.; Arando, M.; García, J. N.; Monforte, A.; Hidalgo, Y. M.; Perez, R. H.; Romero, L. C. Viral Dynamics in Patients with Monkeypox Infection: A Prospective Cohort Study in Spain. *Lancet Infect. Dis.* **2023**, *23* (4), 445−453.
(27) Li, Y.; Olson, V. A.; Laue, T.; Laker, M. T.; Damon, I. K. Detection of Monkeypox Virus with Real-Time PCR Assays. *J. Clin. Virol.* **2006**, *36* (3), 194−203.
(28) Wang, Q.; Liu, M.; Zhao, J.; Yuan, J.; Li, S.; Liu, R. Development of a Magnetic α-Fe2O3/Fe3O4 Heterogeneous Nanorod-Based Electrochemical Biosensing Platform for HPV16 E7 Oncoprotein Detection. *Int. J. Biol. Macromol.* **2025**, *284* (P1), 138085.
(29) Yue, Y.; Liu, M.; Ma, M.; Xu, Z.; Zhang, H.; Wang, Q.; Liu, R. CRISPR/Cas14a Integrated with DNA Walker Based on Magnetic Self-Assembly for Human Papillomavirus Type 16 Oncoprotein E7 Ultrasensitive Detection. *Biosens. Bioelectron.* **2025**, *272* (December 2024), 117135.
(30) Li, Z.; Su, X.; Lin, Y.; Zhang, Y.; Zhang, A.; Wu, X.; Jiyu, X.; Li, Q.; Wei, Z. Expanding the Cell Quantity of CRISPR/Cas9 Gene Editing by Continuous Microfluidic Electroporation Chip. *Bioelectrochemistry* **2025**, *161* (October 2024), 108840.
(31) Huang, X.; Xiao, F.; Jia, N.; Sun, C.; Fu, J.; Xu, Z.; Cui, X.; Huang, H.; Qu, D.; Zhou, J.; Wang, Y. Loop-Mediated Isothermal Amplification Combined with Lateral Flow Biosensor for Rapid and Sensitive Detection of Monkeypox Virus. *Front. Public Heal.* **2023**, *11* (March), 1132896.
(32) Feng, J.; Xue, G.; Cui, X.; Du, B.; Feng, Y.; Cui, J.; Zhao, H.; Gan, L.; Fan, Z.; Fu, T.; Xu, Z.; Du, S.; Zhou, Y.; Zhang, R.; Fu, H.; Tian, Z.; Zhang, Q.; Yan, C.; Yuan, J. Development of a Loop-Mediated Isothermal Amplification Method for Rapid and Visual Detection of Monkeypox Virus. *Microbiol. Spectr.* **2022**, *10* (5), 1−8.
(33) Karem, K. L.; Reynolds, M.; Braden, Z.; Lou, G.; Bernard, N.; Patton, J.; Damon, I. K. Characterization of Acute-Phase Humoral Immunity to Monkeypox: Use of Immunoglobulin M Enzyme-Linked Immunosorbent Assay for Detection of Monkeypox Infection during the 2003 North American Outbreak. *Clin. Vaccine Immunol.* **2005**, *12* (7), 867−872.
(34) Halvaei, P.; Zandi, S.; Zandi, M. Biosensor as a Novel Alternative Approach for Early Diagnosis of Monkeypox Virus. *Int. J. Surg.* **2023**, *109* (1), 50−52.
(35) Garrote, B. L.; Santos, A.; Bueno, P. R. Label-Free Capacitive Assaying of Biomarkers for Molecular Diagnostics. *Nat. Protoc.* **2020**, *15* (12), 3879−3893.
(36) Garrote, B. L.; Lopes, L. C.; Pinzón, E. F.; Mendonça-Natividade, F. C.; Martins, R. B.; Santos, A.; Arruda, E.; Bueno, P. R. Reagentless Quantum-Rate-Based Electrochemical Signal of Graphene for Detecting SARS-CoV-2 Infection Using Nasal Swab Specimens. *ACS Sens.* **2022**, *7* (9), 2645−2653.
(37) Cecchetto, J.; Fernandes, F. C. B.; Lopes, R.; Bueno, P. R. The Capacitive Sensing of NS1 Flavivirus Biomarker. *Biosens. Bioelectron.* **2017**, *87*, 949−956.
(38) Torrente-Rodríguez, R. M.; Lukas, H.; Tu, J.; Min, J.; Yang, Y.; Xu, C.; Rossiter, H. B.; Gao, W. SARS-CoV-2 RapidPlex: A Graphene-Based Multiplexed Telemedicine Platform for Rapid and Low-Cost COVID-19 Diagnosis and Monitoring. *Matter* **2020**, *3* (6), 1981−1998.
(39) de Lima, L. F.; Barbosa, P. P.; Simeoni, C. L.; de Paula, R. F.; Proenca-Modena, J. L.; de Araujo, W. R. Electrochemical Paper-Based Nanobiosensor for Rapid and Sensitive Detection of Monkeypox Virus. *ACS Appl. Mater. Interfaces* **2023**, *15* (50), 58079−58091.
(40) Malard, L. M.; Pimenta, M. A.; Dresselhaus, G.; Dresselhaus, M. S. Raman Spectroscopy in Graphene. *Phys. Rep.* **2009**, *473* (5−6), 51−87.
(41) Pinheiro, T.; Silvestre, S.; Coelho, J.; Marques, A. C.; Martins, R.; Sales, M. G. F.; Fortunato, E. Laser-Induced Graphene on Paper toward Efficient Fabrication of Flexible, Planar Electrodes for

Electrochemical Sensing. *Adv. Mater. Interfaces* **2021**, *8* (22), 2101502.
(42) Stankovich, S.; Dikin, D. A.; Dommett, G. H. B.; Kohlhaas, K. M.; Zimney, E. J.; Stach, E. A.; Piner, R. D.; Nguyen, S. B. T.; Ruoff, R. S. Graphene-Based Composite Materials. *Nature* **2006**, *442* (7100), 282−286.
(43) Goh, M. S.; Pumera, M. Multilayer Graphene Nanoribbons Exhibit Larger Capacitance than Their Few-Layer and Single-Layer Graphene Counterparts. *Electrochem. Commun.* **2010**, *12* (10), 1375−1377.
(44) Morales, D. M.; Risch, M. Seven Steps to Reliable Cyclic Voltammetry Measurements for the Determination of Double Layer Capacitance. *J. Phys. Energy* **2021**, *3* (3), 034013.
(45) Echeverri, D.; Calucho, E.; Marrugo-Ramírez, J.; Álvarez-Diduk, R.; Orozco, J.; Merkoçi, A. Capacitive Immunosensing at Gold Nanoparticle-Decorated Reduced Graphene Oxide Electrodes Fabricated by One-Step Laser Nanostructuration. *Biosens. Bioelectron.* **2024**, *252*, 116142.
(46) Gutierrez, F. A.; Fernandes, F. C. B.; Rivas, G. A.; Bueno, P. R. Mesoscopic Behaviour of Multi-Layered Graphene: The Meaning of Supercapacitance Revisited. *Phys. Chem. Chem. Phys.* **2017**, *19* (9), 6792−6806.
(47) Lehr, J.; Fernandes, F. C. B.; Bueno, P. R.; Davis, J. J. Label-Free Capacitive Diagnostics: Exploiting Local Redox Probe State Occupancy. *Anal. Chem.* **2014**, *86* (5), 2559−2564.
(48) Bueno, P. R.; Feliciano, G. T.; Davis, J. J. Capacitance Spectroscopy and Density Functional Theory. *Phys. Chem. Chem. Phys.* **2015**, *17* (14), 9375−9382.
(49) Garrote, B. L.; Santos, A.; Bueno, P. R. Perspectives on and Precautions for the Uses of Electric Spectroscopic Methods in Label-Free Biosensing Applications. *ACS Sens.* **2019**, *4* (9), 2216−2227.
(50) Marques, S. M.; Santos, A.; Gonçalves, L. M.; Sousa, J. C.; Bueno, P. R. Sensitive Label-Free Electron Chemical Capacitive Signal Transduction for D-Dimer Electroanalysis. *Electrochim. Acta* **2015**, *182*, 946−952.
(51) Holstein, C. A.; Griffin, M.; Hong, J.; Sampson, P. D. Statistical Method for Determining and Comparing Limits of Detection of Bioassays. *Anal. Chem.* **2015**, *87* (19), 9795−9801.
(52) Allegrini, F.; Olivieri, A. C. IUPAC-Consistent Approach to the Limit of Detection in Partial Least-Squares Calibration. *Anal. Chem.* **2014**, *86* (15), 7858−7866.
(53) Allan-Blitz, L.; Carragher, K.; Sukhija-Cohen, A.; Ritchie, P.; Scott, H.; Li, H.; Klausner, J. D. Laboratory Validation and Clinical Performance of a Saliva-based Test for Monkeypox Virus. *J. Med. Virol.* **2023**, *95* (1), No. e28191.
(54) Colavita, F.; Mazzotta, V.; Rozera, G.; Abbate, I.; Carletti, F.; Pinnetti, C.; Matusali, G.; Meschi, S.; Mondi, A.; Lapa, D.; Vita, S.; Minosse, C.; Aguglia, C.; Gagliardini, R.; Specchiarello, E.; Bettini, A.; Nicastri, E.; Girardi, E.; Vaia, F.; Antinori, A.; Maggi, F. Kinetics of Viral DNA in Body Fluids and Antibody Response in Patients with Acute Monkeypox Virus Infection. *iScience* **2023**, *26* (3), 106102.
(55) Pena-Pereira, F.; Wojnowski, W.; Tobiszewski, M. AGREE—Analytical GREEnness Metric Approach and Software. *Anal. Chem.* **2020**, *92* (14), 10076−10082.
(56) Chandran, M.; Chellasamy, G.; Veerapandian, M.; Dhanasekaran, B.; Arumugasamy, S. K.; Govindaraju, S.; Yun, K. Fabrication of Label-Free Immunoprobe for Monkeypox A29 Detection Using One-Step Electrodeposited Molybdenum Oxide-Graphene Quantum Rods. *J. Colloid Interface Sci.* **2024**, *660* (October 2023), 412−422.
(57) Zhou, J.; Xiao, F.; Fu, J.; Jia, N.; Huang, X.; Sun, C.; Liu, C.; Huan, H.; Wang, Y. Rapid Detection of Monkeypox Virus by Multiple Cross Displacement Amplification Combined with Nanoparticle-Based Biosensor Platform. *J. Med. Virol.* **2023**, *95* (2), No. e28479.
(58) Ye, L.; Lei, X.; Xu, X.; Xu, L.; Kuang, H.; Xu, C. Gold-Based Paper for Antigen Detection of Monkeypox Virus. *Analyst* **2023**, *148* (5), 985−994.
(59) Echeverri, D.; Cruz-Pacheco, A. F.; Orozco, J. Capacitive Nanobiosensing of β-1,4-Galactosyltransferase-V Colorectal Cancer Biomarker. *Sensor. Actuator. B Chem.* **2023**, *374*, 132784.

https://doi.org/10.1021/acsaelm.5c00055
ACS Appl. Electron. Mater. 2025, 7, 2882−2893